Status as of August 26, 2026: This is a non-peer-reviewed preprint submitted to EarthArxiv. The manuscript has been submitted for review at Journal of Climate.

Simplified heat budgets can yield misleading diagnoses of ocean temperature change

Noel G. Brizuela,[a] Sarah M. Kang,[a] Malte F. Stuecker,[b,c] Chia-Ying Lee,[d] and Feng Jiang[e]

[a] *Max-Planck Institute for Meteorology, Hamburg, Germany*

[b] *International Pacific Research Center (IPRC), School of Ocean and Earth Science and Technology (SOEST), University of Hawai'i at Mānoa, Honolulu, USA*

[c] *Department of Oceanography, School of Ocean and Earth Science and Technology (SOEST), University of Hawai'i at Mānoa, Honolulu, USA*

[d] *Lamont-Doherty Earth Observatory, Columbia University, New York, USA*

[e] *School of Earth and Environmental Sciences, Seoul National University, Seoul, Republic of Korea*

Corresponding author: Noel G. Brizuela, noel.brizuela@mpimet.mpg.de

ABSTRACT: Temporal changes in upper ocean temperature (T) are crucial indicators of climate variability, change, and its environmental impacts. Ocean heat budgets (OHBs) used to understand these changes are a standard tool across multiple disciplines, but the vast majority of OHBs in published research rely on approximations that are rarely documented and tested. Here, we use output from the CESM2 model to perform exact and approximate OHBs of the Niño3.4 region and compare their results. Exact OHBs are computed using specialized variables that directly reflect the model's implementation of tracer equations, while approximate OHBs use standard variables to recreate the redistribution of heat by oceanic processes. Our results highlight that major drivers of heating can hide within small residual terms and thus go unacknowledged by simplified OHBs. We also find that reconstructions of advective heating exaggerate the role of advection in the growth of ENSO events in this model (by ~25% and ~100% for El Niño and La Niña, respectively). Lastly, we show that eddy parameterizations can dominate multidecadal changes in T and thus represent a poorly-explored source of long-term change. Parameterized processes help shape T across the global ocean, but their contributions go unnoticed in simplified OHBs. To curb incomplete views of the oceanic temperature balance, we propose that future model intercomparison projects save and report values of advective and parameterized heating exactly as implemented by each model.

1. Introduction

Multiscale changes in ocean temperature (T) are among the foremost indicators of regional and global climate change. Variations in T that range from subseasonal to multidecadal timescales are known to have profound impacts on ecosystems, weather, and the hydrological cycle (Soden 2000; Xie et al. 2010; Cavole et al. 2016; Yun et al. 2021; Choi et al. 2024). Diagnosing the drivers of changes in T is therefore a crucial requirement to understanding Earth's future.

Ocean heat budgets (OHBs) are the primary diagnostic method used to understand changes in T. However, ocean variables needed to perform precise OHBs are not included in most data archives, like those associated with model intercomparison projects (MIPs). Atmospheric heat fluxes at the ocean surface are easily available, but the individual heating terms associated with three-dimensional ocean advection and subgrid parameterizations are almost never saved and reported. Without these crucial variables, the vast majority of published OHBs rely on approximations and are left with residuals made up of inaccuracies and true physical processes that cannot be decomposed (Alory and Meyers 2009; Cronin et al. 2015; Keil et al. 2020; Amaya et al. 2020; Tseng et al. 2023; Jiang et al. 2024).

Here, we present a series of comparisons between simplified and exact OHBs to evaluate the effects of typical approximations used in OHB studies. Our analyses are based on output from the Community Earth System model version 2 (CESM2, Danabasoglu et al. 2020) and use the Pacific equatorial region as an example. The results reveal major drawbacks of simplified OHBs in analyses of the upper ocean's i) mean state, ii) interannual variations, and iii) multidecadal warming. All drawbacks are associated to meaningful signals that can hide within residual heating terms and that are necessary to produce a truthful account of the upper ocean heat balance.

The paper is structured as follows. Section 2 reviews the ocean heat equation and compares its precise implementation in ocean models to the simplified formulations used in typical OHBs. Section 3 details the model data and variables used, as well as the primary methods of analysis. Section 4 evaluates the performance of simplified OHBs in analyses of the ocean mean state, its interannual, and multidecadal changes. A discussion in Section 5 reiterates our findings, presents evidence that the pitfalls of simplified OHBs are not unique to the equatorial Pacific region, and argues for the inclusion of specialized heating variables in future model intercomparison projects. Lastly, Section 6 delivers our conclusions.

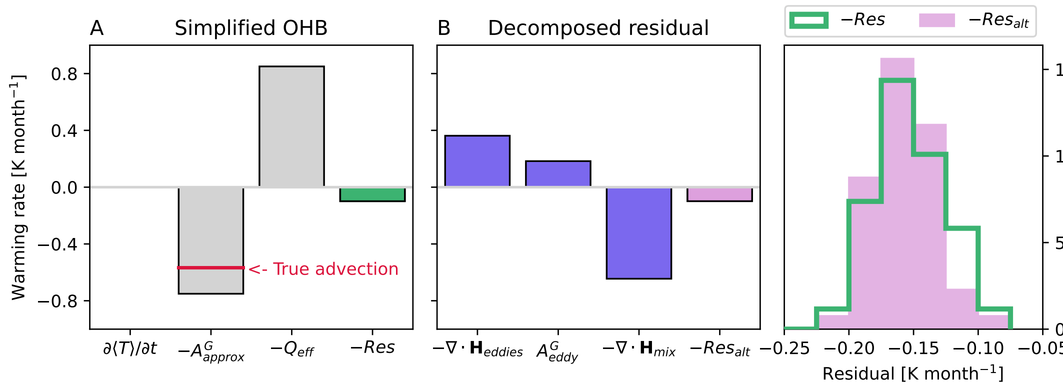

FIG. 1. Two simplified OHBs based on incomplete sets of variables lead to contradictory interpretations. Terms in A) represent a typical approach used in published literature (Eq. 3), where atmospheric heating Q_{eff} and heat advection by the mean circulation A^G_{approx} take priority. In turn, B) decomposes all terms included in the residual Res (Eq. 4). All terms are averaged over an 10-year period between 2020 and 2030 within a coupled simulation of the SSP 585 scenario (see Section 3). Panel C) shows the probability density functions of Res and Res_{alt} using 10-year segments with 50% overlap across our 8 ensemble members (total samples = 7×8).

2. The ocean heat balance

The evolution of $T(x,y,z,t)$ within a three-dimensional flow $\mathbf{u} = (u, v, w)$ follows

$$\frac{\partial T}{\partial t} = -\mathbf{u} \cdot \nabla T - \nabla \cdot \left(\mathbf{Q} + \sum_i \mathbf{H}_i \right), \tag{1}$$

where $\mathbf{Q}$ is a vector including the vertical temperature flux (positive downwards) across the air-sea interface. $\sum_i \mathbf{H}_i$ is the sum of all heat flux vectors associated with individual parameterizations for sub-grid scale mixing and eddies.

Eq. (1) is defined for a continuum, and must be adapted to the discrete grid cells of numerical ocean models. To do so, we integrate $\partial T / \partial t$ over the individual grid cell volumes V_j. Invoking the divergence theorem and the condition of non-divergent flow $\nabla \cdot \mathbf{u} = 0$, we see that $\nabla \cdot (\mathbf{u}T) = \mathbf{u} \cdot \nabla T$. Therefore, we can write

$$\frac{1}{V_j} \int_{V_j} \frac{\partial T}{\partial t} \, dV_j = \frac{-1}{V_j} \int_{\mathbf{S_j}} \hat{n}_j \cdot \left[\mathbf{u}T + \mathbf{Q} + \sum_i \mathbf{H}_i \right] d\mathbf{S}_j, \tag{2}$$

where $\mathbf{S}_j$ is the surface that encloses V_j and $\hat{n}_j$ is a unit vector normal to $\mathbf{S}_j$. Therefore, Eq. (2) tracks changes in T by computing T fluxes that go in and out of an ocean model's grid cell.

a. Simplified formulations

Ocean models can be configured to save output directly from their own implementation of Eq. (2). Doing so allows one to precisely quantify and attribute rates of oceanic heat transfer (Ray et al. 2018). However, this is rarely done and the vast majority of OHBs rely on diagnostic equations that typically read

$$\frac{\partial \langle T \rangle}{\partial t} = -A_{approx} - Q_{approx} - Res. \tag{3}$$

Here, the brackets $\langle \cdot \rangle$ indicate a monthly average and A_{approx} is an estimate of advective heating produced using $\langle \mathbf{u} \rangle$ and $\langle T \rangle$. A_{approx} may be expressed as A^G_{approx} or A^V_{approx} depending on whether it was estimated by computing the advection of gradients $\nabla \langle T \rangle$ or transports $\langle \mathbf{u} \rangle \langle T \rangle$ across the boundaries of a control volume, respectively (see Section 3 for detailed descriptions of these formulations). Furthermore, Q_{approx} makes assumptions about how atmospheric heating is distributed across the upper ocean and may account for a penetrative downward shortwave flux. Lastly, Res is a residual that includes contributions from parameterized heat fluxes $\mathbf{H}_i$ bundled with all errors arising from differences between the diagnostic Eq. (3) and a model's actual implementation of Eq. (2).

Sample values for the top 50 m of the Niño3.4 region (a detailed data description is given in Section 3) exemplify how simplified OHBs may yield seemingly satisfying results but in fact miss important physics (Fig. 1). 10-year average values of all terms in Eq. (3) lead to the familiar conclusion that the Niño3.4 region is heated by the atmosphere and cooled by ocean currents, since Q_{approx} and A^G_{approx} yield tendencies of roughly 0.85 and −0.75 K month^{-1}, respectively (Fig. 1A). We call this a *seemingly satisfying* result because the budget is approximately closed: $\partial \langle T \rangle / \partial t$ is negligible and the term Res carries a cooling tendency −0.10 K / month, much smaller than the main terms Q_{eff} and A_{approx}. Therefore, one could look at Fig. 1A and claim that Q_{eff} and A^G_{approx} are the main drivers of heat transfer in the Niño3.4 region. This leads to the corollary that parameterized and high-frequency processes embedded in *Res do not matter much* to the heat balance of the Niño 3.4 region.

Let us, however, imagine a hypothetical situation in which modeling experiments reported only $\langle T \rangle$ and the exact values of terms bundled within Res. In that case, a simplified OHB would read

$$\frac{\partial \langle T \rangle}{\partial t} = -\nabla \cdot \mathbf{H}_{eddies} - \nabla \cdot \mathbf{H}_{mix} + A_{eddy} - Res_{alt}, \tag{4}$$

where individual fluxes $\mathbf{H}_i$ have been grouped into those arising from parameterizations of ocean eddies ($\mathbf{H}_{eddies}$) and vertical mixing ($\mathbf{H}_{mix}$). Furthermore, the errors associated with $A_{approx} \in \{A^G_{approx}, A^V_{approx}\}$ are given by $A_{eddy} \in \{A^G_{eddy}, A^V_{eddy}\}$, which captures submonthly covariances between $\mathbf{u}$ and T (see Section 3). An alternative residual Res_{alt} now captures all heating terms that are not explicitly included in Eq. (4), namely the sum of A_{approx} and Q_{eff}.

Data available in this alternative scenario leads to the conclusion that the Niño3.4 region is heated by ocean eddies and cooled by vertical mixing (Fig. 1B). During the same 10-year period $-\nabla \cdot \mathbf{H}_{eddies} + A_{eddy}$ and $-\nabla \cdot \mathbf{H}_{mix}$ yield mean tendencies of 0.55 and -0.64 K month^{-1}, respectively, and our residual $-Res_{alt} \approx -0.10$ K month^{-1} has the same magnitude as Res. With this, one could be satisfied, claim that the budget is nearly closed: that eddies and vertical mixing are the primary drivers of heat transfer, while the mean circulation and atmospheric heating do not matter much to the heat balance of the Niño3.4 region.

Two separate OHBs in Fig. 1 describe the same simulation using two different incomplete sets of variables. Blind spots in each approach lead to physical interpretations that seem to contradict each other. We have chosen a decade where $-Res$ and $-Res_{alt}$ are particularly small, but both residuals range between -0.22 and -0.08 K month^{-1} across 56 different 10-year-long segments of our dataset (Fig. 1C). Therefore, whether we use Eq. (3) or (4), we will consistently obtain residual terms that are markedly smaller than the resolved drivers of heat transfer.

Most scientists have become accustomed to think of mean advection and Q_{approx} as the major cooling and heating influences on the Niño3.4 region, but vertical mixing and lateral stirring can play nearly equal roles. Is the balance in Fig. 1A more established than the one in Fig. 1B because it is based on typically-available data, or because it is more physically meaningful?

In reality, the local evolution of T hinges on the interplay of atmospheric heating, advection, and parameterized processes (Menkes et al. 2006; Jochum and Murtugudde 2006; Moum et al. 2013; Ray et al. 2018; Warner and Moum 2019; Deppenmeier et al. 2022). Simplified OHBs that rely

Variable name in CESM2	Description	Notation	Units
SHF	Total vertical heat flux at the ocean surface, positive downwards	$q(z=0)$	W m^{-2}
QSW_3D	Shortwave heat flux across the top of model grid cells	$q(z)$ for $z<0$	W m^{-2}
ADV_3D_TEMP	Temperature tendency caused by resolved ocean advection	$-\mathbf{u}\cdot\nabla T = A_{exact}$	K s^{-1}
TEMP	Temperature	T	°C
UVEL, VVEL, WVEL	Three-dimensional velocities	Components of $\mathbf{u}$	cm s^{-1}
TEND_TEMP	Tendency of thickness-weighted temperature in a model grid cell	$\partial T/\partial t$	K m s^{-1}
ISOP_ADV_TEND_TEMP	Temperature tendency caused by parameterized isopycnal eddies (Gent and Mcwilliams 1990)	Part of $-\nabla\cdot\mathbf{H}_{eddies}$	K s^{-1}
SUBM_ADV_TEND_TEMP	Temperature tendency caused by parameterized submesoscale eddies (Fox-Kemper et al. 2008)	Part of $-\nabla\cdot\mathbf{H}_{eddies}$	K s^{-1}
DIA_IMPVF_TEMP	Temperature flux across the bottom face model grid cells from implicit vertical mixing	Part of $-\nabla\cdot\mathbf{H}_{mix}$	K m s^{-1}
KPP_SRC_TEMP	Temperature tendency caused by non-local mixing in the KPP scheme (Large et al. 1994)	Part of $-\nabla\cdot\mathbf{H}_{mix}$	K s^{-1}
Redi_TEND_TEMP	Temperature tendency caused by Redi diffusion	Part of $-\nabla\cdot\mathbf{H}_{eddies}$	K s^{-1}

TABLE 1. List of CESM2 variables used in the analysis analysis. All variables were saved as monthly averages on the three-dimensional grid. The only exception is SHF, which is two-dimensional and reported at the ocean surface.

on standard output variables will never yield a truthful view of this balance. Even when heating residuals are small, it may be that unquantified processes cancel each other and give us a false sense of confidence. As we will show below, such misleading situations emerge in practical problems across multiple timescales.

3. Data and methods

OHBs presented below aim to diagnose the drivers of mean, interannual, and multidecadal features in T. We use output between years 2015 and 2060 from 8 separate simulations of the SSP5-8.5 emissions scenario made using the Community Earth System Model v2 (CESM2, Danabasoglu et al. 2020). The model output is a subset of control runs presented before by Zhuo et al. (2025). The model's ocean component has a 1° horizontal resolution, but meridional grid spacing reaches roughly 0.25° near the equator. Multiple specialized variables (Table 1) are saved and analyzed to reflect the model's direct implementation of Eq. (2). This way, we repeatedly make comparisons between the insight one can draw from simplified OHBs based on standard output variables, and find when those methods fall short. Unless noted otherwise, all heat budgets presented here are performed on the top 50 m of the Niño3.4 region, which include 5 model layers of 10 m thickness each.

Atmospheric heat fluxes $\mathbf{q} = (0, 0, q)$ are vertical and positive into the ocean. They include radiative, sensible, and latent components whose convergence induces a local warming rate $-\nabla \cdot \mathbf{Q} = -\frac{\partial q}{\partial z}(\rho C_p)^{-1}$. Roughly 4 W m^{-2} of simulated shortwave radiation pass through the bottom (50 m depth) of our study region, representing nearly 5% of the shortwave flux at the surface. This penetrative flux is saved as a 3D field under the name QSW_3D and included in estimates of $-Q_{eff} = -\nabla \cdot \mathbf{Q}$ throughout the text. Therefore, all values of atmospheric heating shown in this manuscript are exact and thus help keep our focus on purely oceanic processes.

We evaluate two methods of estimating oceanic advective heating based on the standard output variables representing $\langle \mathbf{u} \rangle$ and $\langle T \rangle$ (Table 1). First, we recreate the notation in Eq. (1) to write

$$\begin{aligned} \langle \mathbf{u} \cdot \nabla T \rangle &= A^G_{approx} + A^G_{eddy} \\ &= \langle \mathbf{u} \rangle \cdot \nabla \langle T \rangle + A^G_{eddy}, \end{aligned} \tag{5}$$

where A^G_{approx} is our estimate and A^G_{eddy} is a residual that captures submonthly covariance between $\mathbf{u}$ and T, while the superscript G indicates that we've used the 3D gradients of $\langle T \rangle$. Alternatively, one can define a volume of interest $\tilde{V}$ and estimate the mean divergence of temperature transport across its bounding surface $\tilde{\mathbf{S}}$. With this, we replicate the form of Eq. (2) as

$$\begin{aligned} \frac{1}{\tilde{V}} \int_{\tilde{\mathbf{S}}} \hat{n} \cdot \langle \mathbf{u} T \rangle \, d\tilde{\mathbf{S}} &= A^V_{approx} + A^V_{eddy} \\ &= \frac{1}{\tilde{V}} \int_{\tilde{\mathbf{S}}} \hat{n} \cdot \langle \mathbf{u} \rangle \langle T \rangle \, d\tilde{\mathbf{S}} + A^V_{eddy}, \end{aligned} \tag{6}$$

where A^V_{eddy} is again a residual and the superscript V implies that terms are associated to a predetermined volume. In our case, the volume V is bound by the bottom of the fifth model layer

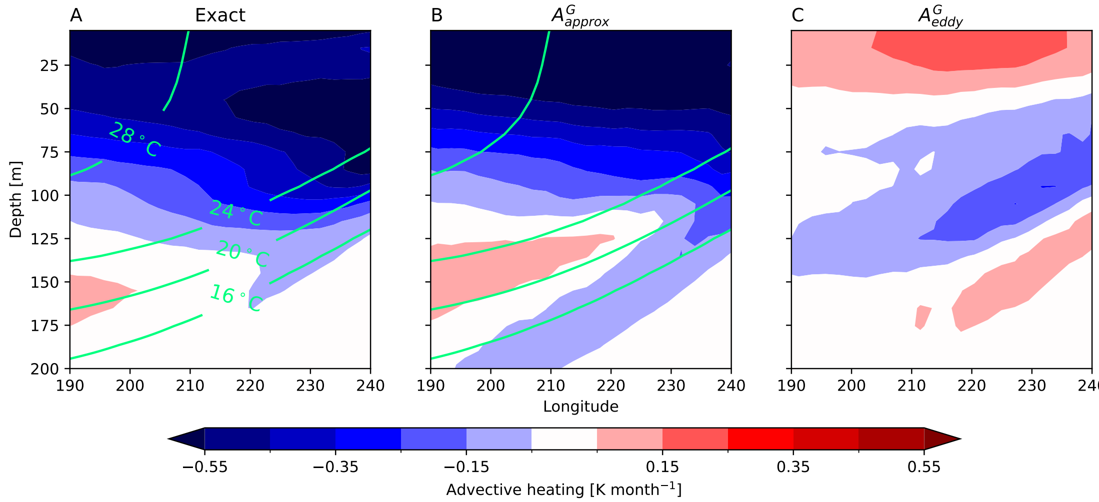

FIG. 2. Estimates of advective heating overestimate the circulation's role in cooling the ocean surface. Meridional and temporal averages of advective heating are shown for A) exact values, B) the gradient-based estimate A^G_{approx} (Eq. 5), and C) their difference A^G_{eddy}. Green contours show the mean locations of the 16, 20, 24, and 28°C isotherms. All values are averaged over 45 years from a single simulation.

and the edges of the Niño 3.4 region at 5°S, 5°N, 190°E, and 240°E. Eddy residuals A^G_{eddy} and A^V_{eddy} are computed by taking the difference between exact values of oceanic advective heating (saved as ADV_3D_TEMP) and the corresponding approximations.

Temperature tendencies associated with parameterized eddies are saved as three separate variables, but we report their sum as $-\nabla \cdot \mathbf{H}_{eddies}$ (Table 1). Lastly, tendencies from parameterized vertical mixing is reported as the sum $-\nabla \cdot \mathbf{H}_{mix}$. Our configuration of CESM2 uses the KPP scheme (Large et al. 1994), which includes two mixing terms. However, our model output only includes the tendency associated with the vertical diffusive flux (DIA_IMPVF_TEMP), and the effects of non-local fluxes (KPP_SRC_TEMP) are inferred indirectly. To do so, we rearrange Eq. (2) to isolate the two mixing flux components and equate them to all other terms, which are known exactly.

Our configuration of CESM2 uses the Parallel Ocean Program 2 (POP2, Smith et al. 2010) as its ocean component. POP2 has a staggered horizontal B-grid, meaning that T is resolved at the center of grid cells while horizontal velocity components u, v are defined at cell corners. The model's advection scheme uses this spatial offset to define finite-difference operations that ensure tracer conservation.

When analyzing output to calculate A^G_{approx} or A^V_{approx}, one can either i) meticulously replicate a model's own schemes as outlined in technical documentation, or ii) further simplify the OHB by using more convenient finite difference schemes. Here, we use the latter option to represent what we believe is perhaps the more common practice. In particular, we implement Eqs. (5) and (6) by first interpolating $\langle \mathbf{u} \rangle$ and $\langle T \rangle$ to a common grid. We further compute gradients $\nabla \langle T \rangle$ by center differences and interpolate transports $\langle \mathbf{u} \rangle \langle T \rangle$ onto the edges of the Niño 3.4 region.

4. Performance of simplified OHBs

a. Estimates of advective heating

Ocean advective cooling in is greater near the eastern edge of the Niño 3.4 region and peaks near 50 m depth (Fig. 2A). Offline estimates A^G_{approx} yield the same peak tendencies of roughly −0.6 K month^{-1} but produce a different spatial pattern, with a weaker zonal contrast and the greatest cooling happening at the surface (Fig. 2B). The difference A^G_{eddy} between reconstructed and exact values changes sign near 50 m depth, meaning that A^G_{approx} tends to exaggerate the role of advection in cooling the ocean surface, and underestimate it in the upper thermocline (Fig. 2C).

Both estimates A^G_{approx} and A^V_{approx} tend to exaggerates the role of advection in cooling the upper 50 m of the Niño3.4 region, yet manage to capture broad patterns of temporal variability (Fig. 3A). Exact output of advective heating yields a mean tendency −0.55 K month^{-1} across our entire dataset of 8 simulations, but Eqs. (5) and (6) yield values −0.68 and −0.80 K month^{-1}, respectively (Fig. 3C). Therefore, values of A^G_{eddy} and A^V_{eddy} account for net heating at mean rates of 0.13 and 0.25 K month^{-1} (Figs. 3B,C).

Time series of A^G_{approx} yield values closer to the true simulated advective heating across our simulations (Fig. 3C). However, this does not necessarily mean that Eq. (5) should be favored over Eq. (6). Estimates A^G_{approx} and A^V_{approx} are shaped by the use of monthly-averaged values, but also by the simplifications of grid geometry and discrete difference operators made during post-processing (see Data and methods). Submonthly covariance between $\mathbf{u}$ and T must play some role in regulating heat advection, and there is no obvious way to tell whether the associated tendency should be that given by A^G_{eddy} or A^V_{eddy}.

Overall, estimates based on Eqs. (5) and (6) can capture broad patterns of variability in advective ocean heating. However, their numerical values should not be understood to indicate the true role of advection in sustaining the local ocean heat balance (Fig. 3C). The contribution of submonthly processes is only knowable when specialized output like ADV_3D_TEMP is available, but even then results can be tremendously sensitive to simplifications of grid geometry: Eqs. (5) and (6) are mathematicall equivalent given $\nabla \cdot \mathbf{u} = 0$, but they yield different values in Fig. 3B because one estimate simplifies gradient operations, while the other one depends only on the interpolation of $\mathbf{u}$ and T to the edges of the Niño3.4 region. In either case, terms A^G_{eddy} and A^V_{eddy} often yield tendencies larger than 0.5 K month^{-1}, sufficient to trigger an El Niño event within months.

Lateral stirring by tropical instability waves (TIWs) are likely contributors to the net heating tendency quantified by A^G_{eddy} and A^V_{eddy}. TIWs enable heat transfer across meridional SST gradients north of the Cold Tongue region, but this effect can not be truthfully captured by monthly means of $\mathbf{u}$ and T (Vialard et al. 2001; Jochum and Murtugudde 2006; Menkes et al. 2006). Still, some studies have argued that eddy terms may be ignored in many model studies because TIWs have small-scale features that ocean models with horizontal resolution $\sim$ 100 km cannot resolve (DiNezio et al. 2009). This justification is not valid for the current generation of climate models, which often include realistic TIWs (Wengel et al. 2021; Moon et al. 2025). For instance, maps of submonthly kinetic energy in our CESM2 simulations a have local maximum that is slightly north of the equator and spans much of the central-eastern Pacific ocean (Fig. S1), a hallmark sign of TIW activity. Likewise, clear evidence of TIWs appears in daily values of SST and advective heating (Fig. S2) as simulated by the Energy Exascale Earth System Model version 3 (E3SM v3.0, Golaz et al. 2026).

b. ENSO cycles

Let us now contextualize the limitations of simplified OHBs in studies of climate variability. To do so, we decompose $T = \tilde{T} + \mathcal{T}$ into its seasonal cycle ($\tilde{T}$) and deviations ($\mathcal{T}$) from it. We compute $\tilde{T}$ by fitting a linear trend and 5 sine waves with periods 12, 6, 4, 3, and 2 months by least squares. $\mathcal{T}$ thus captures all variability in T that is not captured by $\tilde{T}$. Repeating this decomposition for all

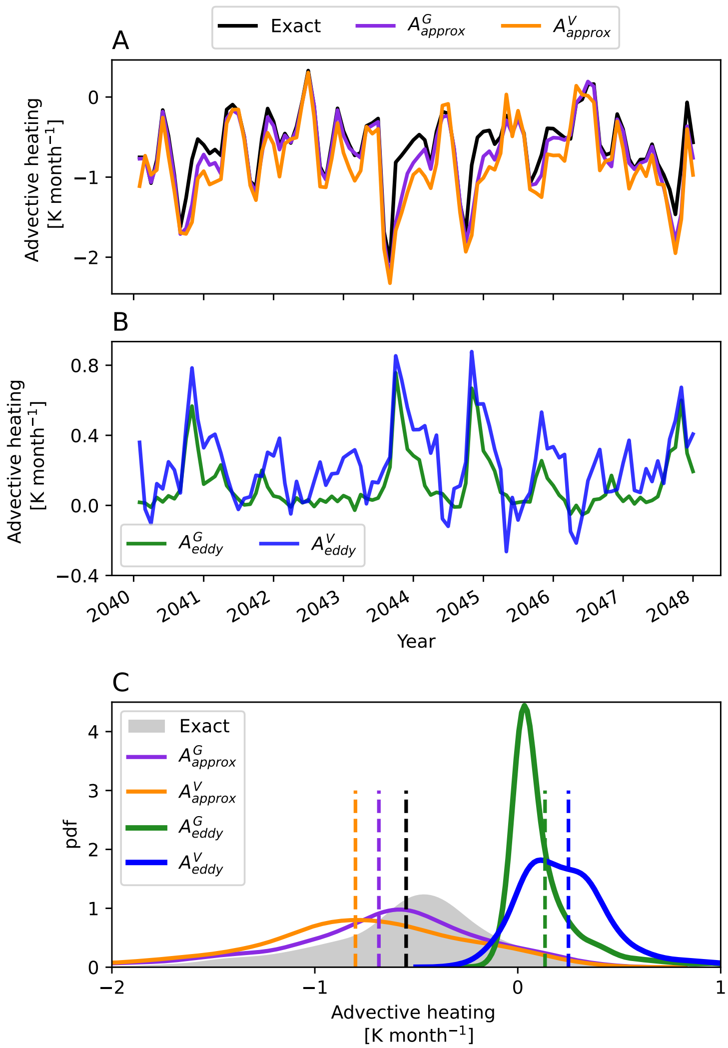

FIG. 3. Estimates A^V_{approx} yield a biased view of advective heating in the Niño3.4 region. Time series in A) show exact and estimated values of advective heating over 8 years of simulation in a single ensemble member. B) are monthly values of the contribution A^V_{eddy} by submonthly advection missed by A^V_{approx}. C) shows non-parametric kernel density estimates of all terms, aggregated over all 8 ensemble members for a total 360 simulation years. Vertical dashed lines in C) are color-coded to indicate the mean value of each distribution. Values calculated for the ocean's top 50 m.

terms in Eq. (1) allows us to write

$$\begin{aligned}\frac{\partial \tilde{T}}{\partial t} + \frac{\partial \mathcal{T}}{\partial t} = &- (\tilde{A}_{approx} + \tilde{A}_{eddy}) \\ &- (\mathcal{A}_{approx} + \mathcal{A}_{eddy}) \\ &- \nabla \cdot \left[\tilde{\mathbf{Q}} + \mathcal{Q} + \sum_i (\tilde{\mathbf{H}}_i + \mathcal{H}_i) \right].\end{aligned} \tag{7}$$

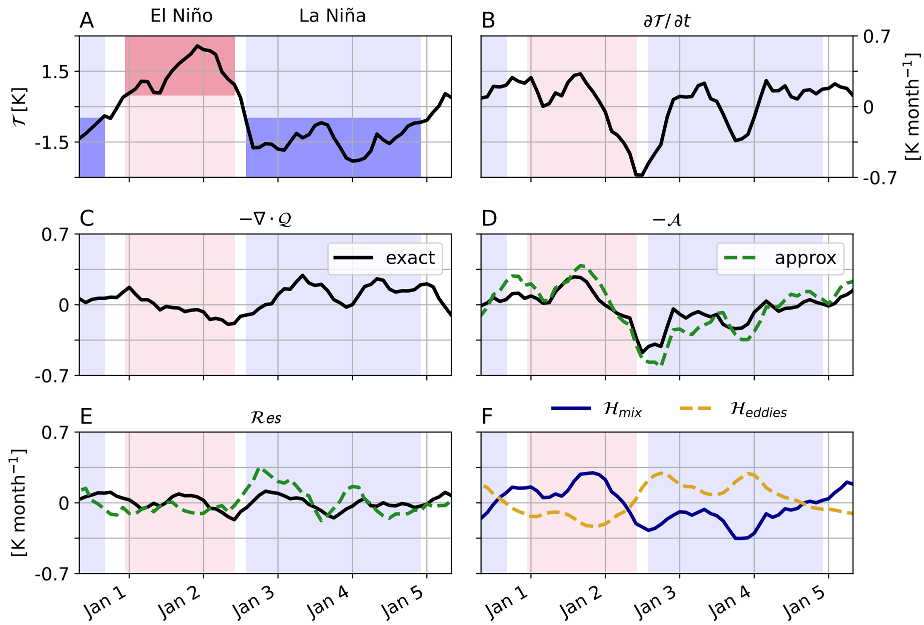

FIG. 4. Two different heating terms can separately explain the timing and magnitude of ENSO events. A succession of El Niño and La Niña events are revealed by A) deviations $\mathcal{T}$ and the anomalous warming rate B) $\partial\mathcal{T}/\partial t$. Atmospheric heating C) $-\nabla\cdot\mathcal{Q}$ alone cannot capture the evolution of $\mathcal{T}$, but either one of D) advective heating and F) parameterized mixing $-\nabla\cdot\mathcal{H}_{mix}$ can. E) shows residuals from simplified OHBs based that consider $\partial\mathcal{T}/\partial t$, $-\nabla\cdot\mathcal{Q}$, and one of the following: (black line) $-\mathcal{A}_{exact}$, (green dashed line $-\mathcal{A}^{V}_{approx}$), or (blue line) $-\nabla\cdot\mathcal{H}_{mix}$. The yellow dashed line in F) shows the contribution from $-\nabla\cdot\mathcal{H}_{eddy}$.

Assuming that all seasonal cycles are balanced among themselves, we are left with an expression for deviations

$$\frac{\partial\mathcal{T}}{\partial t} = -(\mathcal{A}_{approx} + \mathcal{A}_{eddy}) - \nabla\cdot\left(\mathcal{Q} + \sum_i \mathcal{H}_i\right), \qquad (8)$$

where estimates $\mathcal{A}_{approx}$ may be given by Eqs. (5) or (6).

For demonstration purposes, reconstructions of advective heating shown below are based on Eq. (6) only. The supplementary material includes alternative versions of Figs. 4 and 5 that use estimates $\mathcal{A}^{G}_{approx}$ and $\mathcal{A}^{G}_{eddy}$ (Figs. S3, S4) and show that our results are insensitive to the choice of advective heating reconstruction. Standard practice indicates that warm anomalies $\mathcal{T}$ must be sustained for 3-6 months for an ENSO event to be declared (Hanley et al. 2003). Therefore, after calculating deviations from the seasonal cycle, we filter all anomaly terms using a 5-month rolling mean. Our results remained mostly unchanged when analyses were performed using a 3-month rolling mean (not shown).

Our goal now is to determine whether a simplified OHB can reliably explain the occurrence of El Niño and La Niña events. To start, a 5-year long sample of $\mathcal{T}'$ (Fig. 4A) reveals a succession of events and transitions between them. To find a satisfying explanation, we seek a combination of heating terms that can roughly recreate the temporal evolution of $\partial\mathcal{T}'/\partial t$ in Fig. 4B. Throughout much of the period considered here, anomalies $-\nabla\cdot\mathbf{Q}'$ had the same sign as $\partial T'/\partial t$, but their absolute magnitude was clearly too small to explain most of the changes in $\mathcal{T}'$ (Fig. 4C).

Visual inspection of $\mathcal{A}^V_{approx}$ suggests that ocean advection was the primary driver of ENSO events and their transitions, since the reconstructed time series in Fig. 4D closely resembles the net warming $\partial\mathcal{T}/\partial t$ (Fig. 4B). If performing a simplified OHB, one could very easily deem this to be a satisfying answer: the residual left over from adding $\partial\mathcal{T}/\partial t + \nabla\cdot Q + \mathcal{A}^G_{approx}$ (dashed green line in Fig. 4E) oscillates around 0 and mostly opposes $\partial\mathcal{T}/\partial t$.

If one had access to specialized output to compute $\mathcal{A}^G_{eddy}$, one could likely become more confident that variations in advective heating drove the evolution of ENSO events in Fig. 4. The sum $\mathcal{A}^V_{approx} + \mathcal{A}^V_{eddy}$ has weaker variations than the estimate $\mathcal{A}^V_{approx}$ (Fig. 4D), indicating that $\mathcal{A}^V_{eddy}$ acted against the thermal effects of lower-frequency ocean advection. However, accounting for $\mathcal{A}^V_{eddy}$ makes the residual (black line in Fig. 4E) even smaller. With this, whether we reconstruct advective heating values with Eq. (6) or use exact specialized output, we are led to the conclusion that ENSO events were driven by simulated ocean currents.

Interpretation of events in Fig. 4 becomes more complicated upon reviewing time series of $-\nabla\cdot\mathcal{H}_{eddies}$ and $-\nabla\cdot\mathcal{H}_{mix}$ (Fig. 4F). These specialized variables reveal that residuals in Fig. 4E were small not because parameterized processes could be neglected, but because they were strongly anticorrelated. This anticorrelation is physically meaningful and not an artifact of modeling schemes: Theory, observations, and models all indicate that advective heating by the mean flow, near-equatorial eddies, and vertical mixing are all interdependent process that scale with the strength of the trade winds and of the equatorial current system (e.g. Yu et al. 1995; Menkes et al. 2006; Moum et al. 2013; Warner and Moum 2019; Cherian et al. 2021; Moum et al. 2023; Wang et al. 2024).

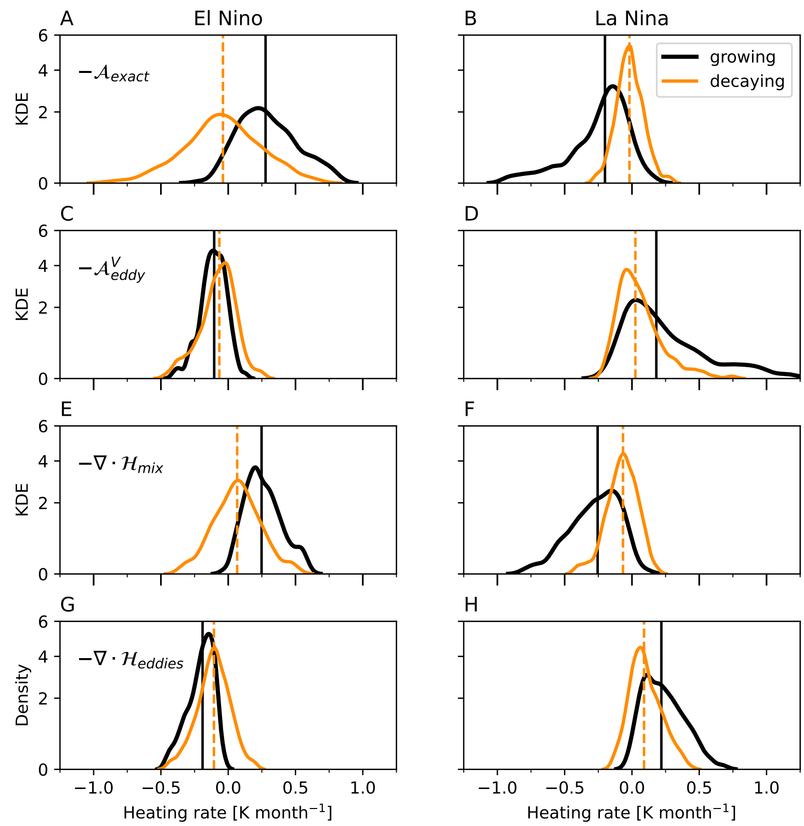

FIG. 5. Probability density functions of anomalous heat budget terms (Eq. 8) in the (black) growing and (orange) decaying phases of (left column) El Niño and (right column) La Niña. The top rows show (A,B) exact values of $-\mathcal{A}_{exact} = -\mathcal{A}^V_{approx} - \mathcal{A}^V_{eddy}$, while (C,D) represent the submonthly contribution $-\mathcal{A}^V_{eddy}$ according to Eq. (6). Panels E and F show contributions from $-\nabla\cdot\mathcal{H}_{mix}$, and (G,H) include $-\nabla\cdot\mathcal{H}_{eddies}$. All values are computed in the Niño3.4 region, and averaged over the ocean's top 50 m. Data is aggregated for 360 simulation years across all 8 ensemble members and includes 104 and 106 individual realizations of El Niño and La Niña, respectively. All plots use a non-linear scaling in the y axis to enhance the visibility of low density values. Vertical lines show the mean values of each distribution.

The time series of $-\nabla\cdot\mathcal{H}_{mix}$ (blue line in Fig. 4F) broadly resembles patterns in $\partial\mathcal{T}/\partial t$ and in the advective term. Therefore, a scientist performing OHBs using output of $-\nabla\cdot\mathcal{H}_{mix}$ rather than $\mathcal{A}^V_{approx} + \mathcal{A}^V_{eddy}$ could easily conclude that ENSO events in Fig. 4 were driven by vertical mixing and not ocean currents.

The notion that ENSO events are driven by anomalies in $-\nabla\cdot\mathcal{H}_{mix}$ resonates with a growing body of observational and modeling literature that details long-term variations in ocean turbulence

(Moum et al. 2013; Warner and Moum 2019; Deppenmeier et al. 2022; Liu et al. 2025). However, the same idea might stand awkwardly in the face of most simplified OHBs and classical works that argue for the dominant role of large scale advection (Philander and Hurlin 1988; Jin et al. 2003; Huang et al. 2012). The truth is that both advection and mixing shaped the evolution of $\mathcal{T}$ in Fig. 4, but the respective roles of each process can only be diagnosed when the complex signals that hide within residuals are decomposed and analyzed.

Parameterized processes and $-\mathcal{A}^{V}_{eddy}$ played key roles shaping ENSO events across our entire dataset. Kernel density estimates in Fig. 5 aggregate data from our entire 360 years of simulations, which include 210 individual ENSO events. This statistical view of heating terms associated with specialized output variables shows that

- $-\nabla \cdot \mathcal{H}_{mix}$ made equal or greater contributions to ENSO phase growth than advective heating (Figs. 5A,B,E,F), and
- anomalies in resolved and parameterized eddies persistently acted to cool the Niño3.4 region during El Niño events (Figs. 5C,G), and warm it during La Niña (Figs. 5D,H).

$-\nabla \cdot \mathcal{H}_{eddies}$ tends to drive tendencies that oppose $-\nabla \cdot \mathcal{H}_{mix}$ (Figs. 4F and 5E-H). Therefore, parameterized eddies and mixing may separately drive heating rates ± 0.25 K month^{-1} in the growing phases of ENSO events but their aggregated effects (solid black line in Fig. 4E) turn out to be quite small. One could understand this systematic relationship to mean that $-\nabla \cdot \mathcal{H}_{eddies}$ canels $-\nabla \cdot \mathcal{H}_{mix}$ and argue that advection (which also drives tendencies $\pm$ 0.25 K month^{-1}) is enough to explain ENSO events. However, one could use the same exact arguments to claim that $-\nabla \cdot \mathcal{H}_{eddies}$ cancels $-\mathcal{A}$ and ENSO events are ultimately driven by $-\nabla \cdot \mathcal{H}_{mix}$.

Again, we have shown that one can reach different conclusions depending on which incomplete set of variables is used to perform a simplified OHB. The reality is that all heating terms collectively shape T in ocean models, but the published literature tends to focus on heating terms that can be quantified using standard output.

c. Multidecadal changes

Having demonstrated the pitfalls of simplified OHBs when assessing the drivers of the equatorial mean state and interannual variability, we now turn our attention to the diagnosis of multidecadal changes in T. Multidecadal OHBs have proliferated in studies of the *pattern effect*, which investigate how spatial patterns in SST change regulate the climate response to radiative forcing by greenhouse gases (Stevens et al. 2016; Armour et al. 2024). Recent work within this community has largely focused on a persistent trend of cooling in the eastern tropical Pacific (Watanabe et al. 2024). This cooling trend is largely missing from CMIP-class climate models (Byrne et al. 2025; Kang et al. 2026) and has thus renewed interest on the mechanisms shaping the ocean temperature balance.

Multidecadal OHBs pose unique challenges, since they aim to diagnose tendencies of the order 0.25 K decade^{-1} (2×10^{-3} K month^{-1}), roughly 400 times smaller than the heating terms that sustain the mean state (Fig. 1). By now, a method laid out by Xie et al. (2010) is perhaps the most popular approach to tackle this challenge. Their approach begins by defining a multidecadal time interval (t_0, t_1) and then computing multi-year averages of terms in Eq. (3) at the beginning and end of that period. In what follows, we use the operator δ to note such a comparison, which is formally defined as

$$\delta := \frac{1}{P}\int_{t_1-P}^{t_1} dt - \frac{1}{P}\int_{t_0}^{t_0+P} dt. \tag{9}$$

Here, P is the length of averaging periods at the beginning and end of the time series being considered. Xie et al. (2010) exemplified this approach setting P to 5 and 10 years when analyzing output from two different simulation ensembles spanning $t_1 - t_0 = 55$ and 60 years, respectively.

Let us then apply δ to both sides of the exact formulation Eq. (1) to obtain

$$\delta\frac{\partial T}{\partial t} = -\delta(A_{approx} + A_{eddy}) - \nabla\cdot\left(\delta\mathbf{Q} + \sum_i \delta\mathbf{H}_i\right), \tag{10}$$

where the term $\delta\partial T/\partial t$ compares concurrent warming rates during the two averaged periods $(t_0, t_0 + P)$ and $(t_1 - P, t_1)$, rather than the mean warming across the entire duration (t_0, t_1). Therefore, $\delta\partial T/\partial t$ and the heating terms that explain it will be primarily shaped by interannual variability whose influence will only diminish as P grows or multiple ensemble members are considered. Furthermore, Eq. (10) can be related to δT only through a series of approximations, as first laid out by Xie et al. (2010). Detailed evaluations of those approximations are available elsewhere (Zhang and Li 2014; Danielli et al. 2025). Hence, we focus on how specialized OHB variables (or the lack thereof) influence the interpretation of analyses based on Eq. (10).

Standard variables included in CMIP repositories only allow rather precise estimation of terms $\delta\partial T/\partial t$ and $\delta\mathbf{Q}$ in Eq. (10). One may estimate δA^G_{approx} or δA^V_{approx} through Eqs. (5) or (6). As

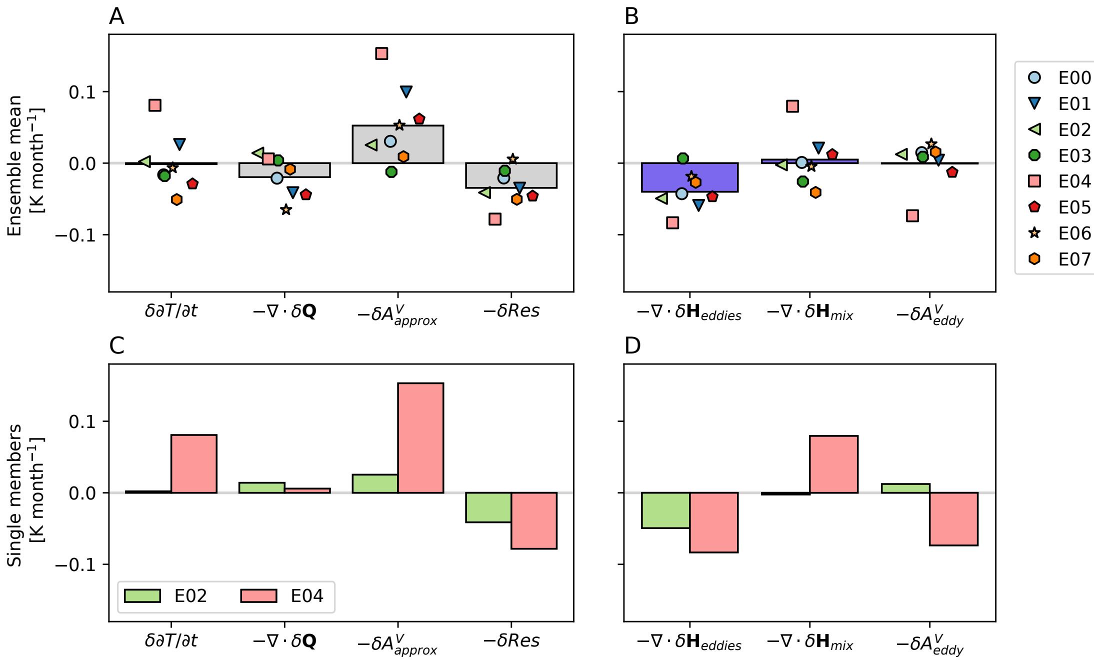

FIG. 6. Multidecadal changes in the Niño 3.4 region, as quantified through simplified (left column) and precise (right column) OHBs. Panels A) and B) show ensemble means of terms in Eqs. (11) and (12) from 8 separate CESM2 model runs. Values corresponding to each individual run are shown using colored markers, while C) and D) show changes from a single ensemble member (ENS04). Changes δ are defined in Eq. (9) and quantified using $P = 10$ years and $t_1 - t_0 = 40$ years.

a result, a residual term will group together contributions from δA^G_{eddy} or δA^V_{eddy}, and $\delta \mathbf{H}_i$. This leaves us with the de-facto balance underlying most multidecadal OHBs

$$\delta \frac{\partial \langle T \rangle}{\partial t} = -\delta A_{approx} - \nabla \cdot (\delta \mathbf{Q}) - \delta Res, \tag{11}$$

where the residual is

$$\delta Res = \delta A_{eddy} + \nabla \cdot (\delta \mathbf{H}_{eddies} + \delta \mathbf{H}_{mix}) + \epsilon \tag{12}$$

and may not be decomposed unless specialized output is available (see Table 1). The term ϵ includes any minor imprecisions that may arise from approximations of $\delta \partial T/\partial t$ and $\delta \mathbf{Q}$, but we do not address it further.

Terms in Eqs. (11) and (12) were quantified in 8 separate CESM2 realizations of the SSP5-8.5 emissions scenario (Fig. 6). Our analysis spans the first 40 years of simulations, such that t_0 is

January 1 of 2015 and t_1 is December 31 of 2054, and P was set to 10 years. Therefore, our analysis considers a different emissions scenario and overall duration than Xie et al. (2010), but is representative of how their method has been adopted and replicated in the research community.

Ensemble mean values of simplified OHB terms show that δA^V_{approx} changed to supply excess heat to the Niño 3.4 area, while that heating was balanced by anomalous cooling from δRes and, to a lesser extent, $\delta \mathbf{Q}$ (Fig. 6A). This leaves us hanging in uncertainty, since the greatest (uncertain) term $\delta A_{approx} \approx 0.052$ K month^{-1} is being balanced primarily by a mysterious oceanic adjustment $\delta Res \approx -0.036$ K month^{-1}. In contrast, the sole two terms that are known with sufficient certainty are relegated to the least important roles, with $-\nabla \cdot \delta \mathbf{Q} \approx -0.015$ K month^{-1} and $\delta \partial T/\partial t \approx -0.001$ K month^{-1}.

Following common practice, one might decide to define $\delta Ocean = \delta A^V_{approx} + \delta Res \approx 0.016$ K month^{-1} and be left with a satisfying, nearly-closed budget. Alternatively, one might try and refine numerical procedures used to estimate δA^V_{approx} or switch to δA^G_{approx} entirely, all in the search for a smaller δRes. Either approach could help minimize δRes, but it will do so without necessarily adding clarity to the physical drivers of changes in the local heat balance.

In our simulations, clarity only comes from knowledge of parameterized heating terms because the ensemble average $-\nabla \cdot \delta \mathbf{H}_{eddies} \approx -0.040$ K month^{-1} was the single greatest term that balanced excess heating (Fig. 6B). Furthermore, consideration of multiple model realizations was crucial, since all terms in Eq. (10) featured an ensemble spread of roughly 0.1 K month^{-1} or greater (Figs. 6A,B). Results from two individual ensemble members in Figs. 6C,D exemplify a simulation whose values are close to the ensemble-average (E02, with negligible $\delta \partial T/\partial t$ and $-\delta Res \approx -\nabla \cdot \delta \mathbf{H}_{eddies}$), and another one that is strongly shaped by transient, interannual signals (E04, with large $\delta \partial T/\partial t$ and non-negligible values in all residual components).

5. Discussion

Simplified OHBs are the primary tool that helps scientists understand changes in T and their relation to components of the climate system. However, missing data and the shortcomings of popular approximations give rise to large unknowns that might mislead scientists (Figs. 4 and 5).

Despite missing data, scientists are often pressed to obtain small values for Res. In practice, this gives the impression that the major processes sustaining T have been identified. When Res is

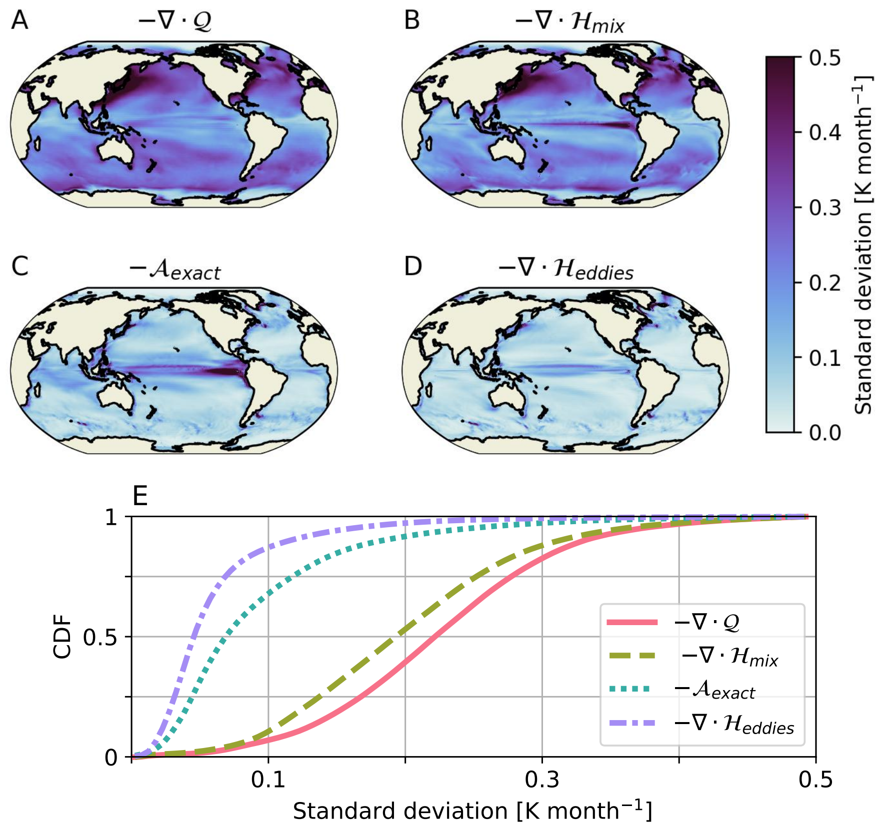

FIG. 7. Standard deviation of yearly-averaged heating terms in Eq. (8) for the ocean's top 50 m across our 8 ensemble members. Global maps show distinct patterns in A) $-\nabla \cdot \mathcal{Q}$, B) $-\nabla \cdot \mathcal{H}_{mix}$, C) $-\mathcal{A}_{exact}$, and D) $-\nabla \cdot \mathcal{H}_{eddies}$. Cumulative density functions in E) show a statistical summary of standard deviation values in panels A-E, which aggregate data from all 8 simulations.

large, however, scientists may be tempted to tinker with computational details until Res becomes small and the budget appears closed. For instance, they may switch between Eqs. (5) and (6), change the control volume $\tilde{V}$ for their study, or modify their management of grid information and numerical implementation of vector operations. These efforts can be time-consuming and lead to analysis iterations before Res becomes small enough or scientists give up. Even with a small Res, however, one can miss a whole set of first-order heating terms that simply add up to a small number (Figs. 1, 4).

Sophisticated parameterizations enable the realism and skill of contemporary ocean models. Despite their major role shaping T (Figs. 5, 6), parameterized processes are rarely included in published OHBs and climate theories. Some studies have sought to infer the role of parameterizations using standard output (Jiang et al. 2025, 2026), but precise diagnoses are only possible when specialized output variables help constrain heating terms (Table 1).

Simplified models, including mixed layer formulations, sometime use implicit assumptions and parameterizations to account for vertical mixing and eddies (Philander and Hurlin 1988; Jin et al. 2003; Cronin et al. 2015). While those methods may yield realistic numerics, they can also give the impression that implicit processes are secondary or non-important. For example, when someone assumes that surface heat fluxes will be evenly distributed across a mixed layer, they are choosing to take for granted specific values for $\mathbf{H}_{mix}$. Similar assumptions are made to relate upwelling and surface T (e.g. Zebiak and Cane 1987). Our results highlight how parameterizations make contributions to $\partial T/\partial t$ that are highly dynamic and may not be well captured by rigid, implicit formulations.

We chose to focus on the top 50 m of the Niño3.4 region because OHBs of this area have been of major interest to the ocean and climate communities for decades. A growing number of studies point to the paramount role of subgrid-scale processes in the local heat balance (Moum et al. 2013; Ray et al. 2018; Warner and Moum 2019; Deppenmeier et al. 2022; Liu et al. 2025; Jiang et al. 2025, 2026), but these lessons may be masked in simplified OHBs. Our results, however, are likely relevant to vast regions of the global ocean (Fig. 7).

Global maps of standard deviations in Fig. 7 help assess the potential contributions of each heating term to interannual variations in T. Standard deviations are calculated after calculating yearly averages and detrending local time series, always averaged for the ocean's top 50 m. The spatial patterns and magnitudes of variations in $-\nabla \cdot Q$ and $-\nabla \cdot \mathcal{H}_{mix}$ closely resemble each other (Figs. 7A,B), indicating that air-sea fluxes and vertical mixing are equally important in diagnosing interannual deviations in T. Variations in $-\mathcal{A}_{exact}$ and $-\nabla \cdot \mathcal{H}_{eddies}$ are weaker in comparison (Figs. 7C-E), but make substantial contributions in near-equatorial regions, western boundary currents, and some regions of the Southern Ocean.

Even though $-\nabla \cdot Q$ and $-\nabla \cdot \mathcal{H}_{mix}$ make the greatest contributions to interannual variations in T, anomalous heating associated with $-\mathcal{A}_{exact}$ and $-\nabla \cdot \mathcal{H}_{eddies}$ is large enough to drive notable events in many regions. Cumulative density functions in Fig. 7E describe the standard deviation of yearly-averaged heating terms and reveal that $-\mathcal{A}_{exact}$ and $-\nabla \cdot \mathcal{H}_{eddies}$ impose anomalous tendencies greater than 0.1 K month^{-1} over roughly 30% and 15% of the ocean surface area, respectively. Considered in isolation, either of such tendencies would drive drastic interannual oscillations in upper ocean T. However, simulated variations in T may be smaller given the interrelated nature of all terms in Eq. (1). This again emphasizes the crucial need for OHBs that consider the potential for major contributions to come from all processes shaping T.

a. A proposal to include specialized variables in MIPs

Model Intercomparison Projects (MIPs) aggregate output from climate simulations developed across dozens of institutions and modeling centers worldwide. All experiments adhere to strict guidelines designed to ensure that inter-model comparisons are physically meaningful and interpretable, reflecting intrinsic differences between climate models rather than arbitrary and subjective details about forcing datasets and initialization routines.

Simplified OHBs may perform better in some climate models than others, but this is no reason to ignore the pitfalls evidenced above. Output from MIPs is routinely analyzed using simplified OHBs (e.g. Danielli et al. 2025; Gopika et al. 2025), but inter-model OHB comparisons are likely influenced by both model-dependent physics and biases associated with how OHB approximations interact with each model's grid and numerical schemes. Differences between estimates A^G_{eddy} and A^V_{eddy} in Fig. 3 exemplify this latter source of variations in analysis: the relation between gradient-based and volume-based formulations of heat advection is formal and exact, but their application in postprocessing may carry spurious biases in practice.

Without standardized output that faithfully reflects how oceanic processes shape T in ocean models, it will be much harder to make sense of inter-model discrepancies published in the MIP literature. We believe that great improvements would come from archiving 3D variables for A_{exact}, $-\nabla \cdot \mathbf{H}_{mix}$, and $-\nabla \cdot \mathbf{H}_{eddies}$. If these tendencies are all saved and reported as implemented in each model, inter-model OHB comparisons will more easily identify differences in model physics that most impact T.

Before readers form an opinion on whether it is worth to store three additional data variables in MIP submissions, we ask them to consider how much effort is spent tinkering with simplified OHBs in the pursuit of small residual terms. Most people who have performed a simplified OHB will be familiar with the painstaking process of validating, interpreting, and trusting results. Archival of additional variables reflecting exact heating rates and their attribution to physical processes will standardize this work and make it streamlined. 3D ocean variables in CMIP6 generally took up between 10 and 15 MB per period saved (typically monthly), so the extra cost in storage may be well worth it.

Mounting observational evidence points to the crucial role of small-scale and transient ocean motions in shaping large-scale ocean properties (Moum et al. 2013; Warner and Moum 2019; Siegelman et al. 2020). Great efforts have been spent parameterizing and resolving these processes and the scale interactions that emerge from them. Simplified OHBs risk undermining such efforts in our interpretation of climate model results and therefore prevent the development of cohesive understanding across research communities. As such, we believe that simplified OHBs come with unintended consequences that are counter to the spirit and goals of MIPs, but specialized output variables can solve the issue.

6. Conclusions

Three-dimensional currents and parameterized subsurface processes regulate T across the global ocean (Fig. 7). Reconstructions of advective ocean heating based on standard output variables $\langle \mathbf{u} \rangle$ and $\langle T \rangle$ miss submonthly covariances that sustain the mean state and help drive interannual variability in the current generation of ocean models (Fig. 3). Simplified OHBs that do not explicitly account for such resolved and parameterized heating terms risk leading to incomplete and misleading diagnoses even if residual terms are small (Figs. 1 and 4).

Understanding the mechanisms of planetary change requires that scientific communities have a common basis to understand the evolution of T. Incomplete physical explanations coming out of simplified OHBs can drive a wedge between scientific communities that study the same region. The major influence of parameterized mixing and eddies in regulating Pacific equatorial T (Figs. 1, 5, 6) serves as an example, but more are likely to exist.

Ocean models can be configured to output the precise values of terms in their own implementation of the ocean heat balance (e.g. Table 1). Such specialized output is rarely available in existing datasets, but can spare researchers dependence on poor approximations. The authors believe that additional clarity gained from precise accounting of heating terms will likely enhance communication between scientific communities and accelerate progress across the fields of oceanography, climate science, and ecosystem dynamics.

Acknowledgments. The authors thank Jing-Yi Zhuo, who performed the control state CESM2 simulations that our analyses are based on. This material is based upon work supported by the U.S. Department of Energy, Office of Science, Office of Biological and Environmental Research, under Award Number DE-SC0025595. This report was prepared as an account of work sponsored by an agency of the United States Government. Neither the United States Government nor any agency thereof, nor any of their employees, makes any warranty, express or implied, or assumes any legal liability or responsibility for the accuracy, completeness, or usefulness of any information, apparatus, product, or process disclosed, or represents that its use would not infringe privately owned rights. Reference herein to any specific commercial product, process, or service by trade name, trademark, manufacturer, or otherwise does not necessarily constitute or imply its endorsement, recommendation, or favouring by the United States Government or any agency thereof. The views and opinions of authors expressed herein do not necessarily state or reflect those of the United States Government or any agency thereof. This is IPRC publication X and SOEST contribution Y.

Data availability statement. Heat budget data and scripts needed to reproduce figures can be found in the Open Research Data Repository of the Max Planck Society EDMOND (doi.org/10.17617/3.M7MDHG)

References

Alory, G., and G. Meyers, 2009: Warming of the upper equatorial indian ocean and changes in the heat budget (1960–99). *Journal of Climate*, **22 (1)**, 93–113, https://doi.org/doi.org/10.1175/2008JCLI2330.1.

Amaya, D. J., A. J. Miller, S.-P. Xie, and Y. Kosaka, 2020: Physical drivers of the summer 2019 north pacific marine heatwave. *Nature communications*, **11 (1)**, 1903, https://doi.org/doi.org/10.1038/s41467-020-15820-w.

Armour, K. C., and Coauthors, 2024: Sea-surface temperature pattern effects have slowed global warming and biased warming-based constraints on climate sensitivity. *Proceedings of the National Academy of Sciences*, **121 (12)**, e2312093 121.

Byrne, H., R. Seager, and J. E. Smerdon, 2025: Cmip6 models cannot capture long-term forced changes in the tropical pacific sea surface temperature gradient. *Nature Communications*.

Cavole, L. M., and Coauthors, 2016: Biological impacts of the 2013–2015 warm-water anomaly in the northeast pacific: winners, losers, and the future. *Oceanography*, **29 (2)**, 273–285.

Cherian, D., D. Whitt, R. Holmes, R.-C. Lien, S. Bachman, and W. Large, 2021: Off-equatorial deep-cycle turbulence forced by tropical instability waves in the equatorial pacific. *Journal of Physical Oceanography*, **51 (5)**, 1575–1593, https://doi.org/doi.org/10.1175/JPO-D-20-0229.1.

Choi, H.-Y., M.-S. Park, H.-S. Kim, and S. Lee, 2024: Marine heatwave events strengthen the intensity of tropical cyclones. *Communications Earth & Environment*, **5 (1)**, 69, https://doi.org/doi.org/10.1038/s43247-024-01239-4.

Cronin, M. F., N. A. Pelland, S. R. Emerson, and W. R. Crawford, 2015: Estimating diffusivity from the mixed layer heat and salt balances in the north pacific. *Journal of Geophysical Research: Oceans*, **120 (11)**, 7346–7362, https://doi.org/doi.org/10.1002/2015JC011010.

Danabasoglu, G., and Coauthors, 2020: The community earth system model version 2 (cesm2). *Journal of Advances in Modeling Earth Systems*, **12 (2)**, e2019MS001 916, https://doi.org/doi.org/10.1029/2019MS001916.

Danielli, V., M. Lengaigne, K. Sadhvi, S. Gopika, and J. Vialard, 2025: Drivers of cmip tropical pacific warming pattern diversity. *Earth's Future*, **13 (8)**, e2025EF005 938.

Deppenmeier, A.-L., F. O. Bryan, W. S. Kessler, and L. Thompson, 2022: Diabatic upwelling in the tropical pacific: Seasonal and subseasonal variability. *Journal of Physical Oceanography*, **52 (11)**, 2657 – 2668, https://doi.org/10.1175/JPO-D-21-0316.1.

DiNezio, P. N., A. C. Clement, G. A. Vecchi, B. J. Soden, B. P. Kirtman, and S.-K. Lee, 2009: Climate response of the equatorial pacific to global warming. *Journal of Climate*, **22 (18)**, 4873–4892.

Fox-Kemper, B., R. Ferrari, and R. Hallberg, 2008: Parameterization of mixed layer eddies. part i: Theory and diagnosis. *Journal of Physical Oceanography*, **38 (6)**, 1145–1165, https://doi.org/doi.org/10.1175/2007JPO3792.1.

Gent, P. R., and J. C. Mcwilliams, 1990: Isopycnal mixing in ocean circulation models. *Journal of Physical Oceanography*, **20 (1)**, 150–155, https://doi.org/doi.org/10.1175/1520-0485(1990)020⟨0150:IMIOCM⟩2.0.CO;2.

Golaz, J.-C., and Coauthors, 2026: The energy exascale earth system model version 3: 2. overview of the coupled system. *Journal of Advances in Modeling Earth Systems*, **18 (4)**, e2025MS005 302.

Gopika, S., K. Sadhvi, J. Vialard, V. Danielli, S. Neetu, and M. Lengaigne, 2025: Drivers of future indian ocean warming and its spatial pattern in cmip models. *Earth's Future*, **13 (4)**, e2025EF006 112.

Hanley, D. E., M. A. Bourassa, J. J. O'Brien, S. R. Smith, and E. R. Spade, 2003: A quantitative evaluation of enso indices. *Journal of Climate*, **16 (8)**, 1249–1258.

Huang, B., Y. Xue, H. Wang, W. Wang, and A. Kumar, 2012: Mixed layer heat budget of the el niño in ncep climate forecast system. *Climate Dynamics*, **39 (1)**, 365–381, https://doi.org/doi.org/10.1007/s00382-011-1111-4.

Jiang, F., R. Seager, and M. A. Cane, 2024: Historical subsurface cooling in the tropical pacific and its dynamics. *Journal of Climate*, **37 (22)**, 5925–5938, https://doi.org/doi.org/10.1175/JCLI-D-24-0007.1.

Jiang, F., R. Seager, and M. A. Cane, 2026: Deus ex machina long-term cooling of the eastern pacific cold tongue in ocean reanalysis data. *Journal of Climate*, **39 (12)**, 3303–3318.

Jiang, F., R. Seager, M. A. Cane, C. Karamperidou, and N. G. Brizuela, 2025: Subsurface cooling and sea surface temperature pattern formation over the equatorial pacific. *Journal of Geophysical Research: Oceans*, **130 (4)**, e2024JC022 222.

Jin, F.-F., S.-I. An, A. Timmermann, and J. Zhao, 2003: Strong el niño events and nonlinear dynamical heating. *Geophysical Research Letters*, **30 (3)**, 20–1, https://doi.org/doi.org/10.1029/2002GL016356.

Jochum, M., and R. Murtugudde, 2006: Temperature advection by tropical instability waves. *Journal of Physical Oceanography*, **36 (4)**, 592–605, https://doi.org/doi.org/10.1175/JPO2870.1.

Kang, S. M., D. A. Putrasahan, N. G. Brizuela, H. Haak, J. Kröger, J. Marotzke, B. Stevens, and J.-S. von Storch, 2026: Km-scale coupled simulation and model–observation sst trend discrepancy. *Proceedings of the National Academy of Sciences*, **123 (8)**, e2522161 123.

Keil, P., T. Mauritsen, J. Jungclaus, C. Hedemann, D. Olonscheck, and R. Ghosh, 2020: Multiple drivers of the north atlantic warming hole. *Nature Climate Change*, **10 (7)**, 667–671, https://doi.org/doi.org/10.1038/s41558-020-0819-8.

Large, W. G., J. C. McWilliams, and S. C. Doney, 1994: Oceanic vertical mixing: A review and a model with a nonlocal boundary layer parameterization. *Reviews of geophysics*, **32 (4)**, 363–403.

Liu, C., F. Wang, A. Köhl, X. Wang, C. Wang, and K. J. Richards, 2025: Subsurface ocean turbulent mixing enhances central pacific enso. *Nature Communications*, **16 (1)**, 2315.

Menkes, C. E., J. G. Vialard, S. C. Kennan, J.-P. Boulanger, and G. V. Madec, 2006: A modeling study of the impact of tropical instability waves on the heat budget of the eastern equatorial pacific. *Journal of Physical Oceanography*, **36 (5)**, 847–865, https://doi.org/doi.org/10.1175/JPO2904.1.

Moon, J.-Y., and Coauthors, 2025: Earth's future climate and its variability simulated at 9 km global resolution. *Earth System Dynamics*, **16 (4)**, 1103–1134, https://doi.org/10.5194/esd-16-1103-2025.

Moum, J. N., A. Perlin, J. D. Nash, and M. J. McPhaden, 2013: Seasonal sea surface cooling in the equatorial pacific cold tongue controlled by ocean mixing. *Nature*, **500 (7460)**, 64–67, https://doi.org/doi.org/10.1038/nature12363.

Moum, J. N., W. D. Smyth, K. G. Hughes, D. Cherian, S. J. Warner, B. Bourlès, P. Brandt, and M. Dengler, 2023: Wind dependencies of deep cycle turbulence in the equatorial cold tongues. *Journal of Physical Oceanography*, **53 (8)**, 1979–1995, https://doi.org/doi.org/10.1175/JPO-D-22-0203.1.

Philander, S., and W. Hurlin, 1988: The heat budget of the tropical pacific ocean in a simulation of the 1982–83 el niño. *Journal of Physical Oceanography*, **18 (6)**, 926–931, https://doi.org/doi.org/10.1175/1520-0485(1988)018⟨0926:THBOTT⟩2.0.CO;2.

Ray, S., A. T. Wittenberg, S. M. Griffies, and F. Zeng, 2018: Understanding the equatorial pacific cold tongue time-mean heat budget. part i: Diagnostic framework. *Journal of Climate*, **31 (24)**, 9965–9985, https://doi.org/doi.org/10.1175/JCLI-D-18-0152.1.

Siegelman, L., P. Klein, P. Rivière, A. F. Thompson, H. S. Torres, M. Flexas, and D. Menemenlis, 2020: Enhanced upward heat transport at deep submesoscale ocean fronts. *Nature Geoscience*, **13 (1)**, 50–55, https://doi.org/doi.org/10.1038/s41561-019-0489-1.

Smith, R., and Coauthors, 2010: The parallel ocean program (pop) reference manual: Ocean component of the community climate system model (ccsm). *Rep. LAUR-01853*, **141**, 1–141.

Soden, B. J., 2000: The sensitivity of the tropical hydrological cycle to enso. *Journal of Climate*, **13 (3)**, 538–549.

Stevens, B., S. C. Sherwood, S. Bony, and M. J. Webb, 2016: Prospects for narrowing bounds on earth's equilibrium climate sensitivity. *Earth's Future*, **4 (11)**, 512–522, https://doi.org/doi.org/10.1002/2016EF000376.

Tseng, H.-Y., Y.-T. Hwang, S.-P. Xie, Y.-H. Tseng, S. M. Kang, M. T. Luongo, and I. Eisenman, 2023: Fast and slow responses of the tropical pacific to radiative forcing in northern high latitudes. *Journal of Climate*, **36 (16)**, 5337–5349, https://doi.org/doi.org/10.1175/JCLI-D-22-0622.1.

Vialard, J., C. Menkes, J.-P. Boulanger, P. Delecluse, E. Guilyardi, M. J. McPhaden, and G. Madec, 2001: A model study of oceanic mechanisms affecting equatorial pacific sea surface temperature during the 1997–98 el niño. *Journal of Physical Oceanography*, **31 (7)**, 1649–1675, https://doi.org/doi.org/10.1175/1520-0485(2001)031⟨1649:AMSOOM⟩2.0.CO;2.

Wang, M., S.-P. Xie, H. Sasaki, M. Nonaka, and Y. Du, 2024: Intensification of pacific tropical instability waves over the recent three decades. *Nature Climate Change*, **14 (2)**, 163–170.

Warner, S. J., and J. N. Moum, 2019: Feedback of mixing to enso phase change. *Geophysical Research Letters*, **46 (23)**, 13 920–13 927, https://doi.org/doi.org/10.1029/2019GL085415.

Watanabe, M., S. M. Kang, M. Collins, Y.-T. Hwang, S. McGregor, and M. F. Stuecker, 2024: Possible shift in controls of the tropical pacific surface warming pattern. *Nature*, **630 (8016)**, 315–324.

Wengel, C., S.-S. Lee, M. F. Stuecker, A. Timmermann, J.-E. Chu, and F. Schloesser, 2021: Future high-resolution el niño/southern oscillation dynamics. *Nature Climate Change*, **11 (9)**, 758–765, https://doi.org/10.1038/s41558-021-01132-4.

Xie, S.-P., C. Deser, G. A. Vecchi, J. Ma, H. Teng, and A. T. Wittenberg, 2010: Global warming pattern formation: Sea surface temperature and rainfall. *Journal of Climate*, **23 (4)**, 966 – 986, https://doi.org/10.1175/2009JCLI3329.1.

Yu, Z., J. P. McCreary Jr, and J. A. Proehl, 1995: Meridional asymmetry and energetics of tropical instability waves. *Journal of Physical Oceanography*, **25 (12)**, 2997–3007.

Yun, K.-S., J.-Y. Lee, A. Timmermann, K. Stein, M. F. Stuecker, J. C. Fyfe, and E.-S. Chung, 2021: Increasing enso–rainfall variability due to changes in future tropical temperature–rainfall relationship. *Communications Earth & Environment*, **2 (1)**, 43.

Zebiak, S. E., and M. A. Cane, 1987: A model el niño–southern oscillation. *Monthly Weather Review*, **115 (10)**, 2262–2278.

Zhang, L., and T. Li, 2014: A simple analytical model for understanding the formation of sea surface temperature patterns under global warming. *Journal of Climate*, **27 (22)**, 8413–8421, https://doi.org/doi.org/10.1175/JCLI-D-14-00346.1.

Zhuo, J.-Y., C.-Y. Lee, A. Sobel, R. Seager, S. J. Camargo, Y.-H. Lin, B. Fosu, and K. A. Reed, 2025: A more la niña–like response to radiative forcing after flux adjustment in cesm2. *Journal of Climate*, **38 (4)**, 1037–1050, https://doi.org/doi.org/10.1175/JCLI-D-24-0331.1.